Inorg. Chem. **2007**, *46*, 417–427

Theoretical Determination of the Excited States and of *g*-Factors of the Creutz–Taube Ion, $[(NH_3)_5–Ru–pyrazine–Ru–(NH_3)_5]^{5+}$

Hélène Bolvin*

Laboratoire de Chimie Quantique, Institut de Chimie de Strasbourg, LC 3 - UMR 7177 4 rue Blaise Pascal 67000 Strasbourg, France

Received May 12, 2006

The Creutz–Taube complex $[(NH_3)_5–Ru–pyrazine–Ru–(NH_3)_5]^{5+}$ is studied using wave function-based methods, namely the CASSCF/MS-CASPT2 method. Spin–orbit effects have been calculated with the SO-RASSI program. The nature of the ground state is analyzed, and all the excited states up to 50 000 cm^{-1} are calculated. They form a quasi continuum from 25 000 cm^{-1}, theoretical bands are assigned to UV–visible spectra, and MCD bands are assigned by calculating transition moments from first principles for both spectroscopies. *g*-Factors are calculated from first principles and modeled by a model Hamiltonian: they compare well to experimental values and are shown to be the same as in the monomeric species.

1. Introduction

Bridged bimetallic systems are very important for the understanding of through-ligand intramolecular electron transfer. The main implications of the current research are in biochemical processes where electron, charge, or energy transfer are often involved and in molecular electronics where electrode−molecule−electrode conduction is studied or where the charge transfer is combined with other physical properties (nonlinear optics, magnetic properties) to obtain devices with tailored properties.

One of the most known bridged mixed-valence molecules is $[(NH_3)_5-Ru-pyrazine-Ru-(NH_3)_5]^{5+}$, which was synthesized and first studied by Creutz and Taube in 1969: it is usually called the Creutz−Taube (CT) ion.[1] In a symmetrical mixed-valence compound, the unpaired electron can be either localized on one metallic center or delocalized on the two metallic centers. There is a competition between electronic coupling between the metallic centers that favors delocalization and geometrical relaxation which may trap the electron on a single center. Whether the electron is localized or not has been the subject of controversy during some decades, and many experimental techniques and theoretical approaches have been applied to this molecule in order to solve this question. It is nowadays accepted that this ion belongs to the class II−III, which means that the unpaired electron is localized on one of the ruthenium but that the electron transfer between the two sites is faster than some relaxation times, specially the ones concerning the solvent.[2] The aim of the present theoretical study is, however, not to answer the question of localization of the excess electron; the CT ion is experimentally and theoretically well studied, we have therefore chosen it as a benchmark molecule to, on one hand, investigate the ability of the CASSCF (complete active space self-consistent field)/CASPT2 (complete active space perturbation theory at the second order) method to describe this type of molecule and, on the other hand, to analyze whether this multireference method provides new understanding of the electronic structure of this ion.

The synthesis of new mixed-valence compounds including bridged dimers of ruthenium is still an active field of research.[3−9] Their properties, in particular the electronic coupling between the metal centers through the bridge, are investigated using electrochemistry, spectroelectrochemistry,

* E-mail: bolvin@chimie.u-strasbg.fr.

(1) Creutz, C.; Taube, H. J. *J. Am. Chem. Soc.* **1969**, *91*, 3988.
(2) Demadis, K. D.; Hartshorn, C. M.; Meyer, T. J. *Chem. Rev.* **2001**, *101*, 2655.
(3) Kaim, W.; Klein, A.; Glöcke, M. *Acc. Chem. Res.* **2000**, *33*, 755.
(4) Flores-Torres, S.; Hutchinson, G. R.; Soltzberg, L. J.; Abruna, H. D. *J. Am. Chem. Soc.* **2006**, *128*, 1513.
(5) Wolpher, H.; Huang, P.; Borgström, M.; Bergquist, J.; Styring, S.; Sun, L.; Åkermark, B. *Catal. Today* **2004**, *98*, 529.
(6) Kar, S.; Chanda, N.; Mobin, S. M.; Datta, A.; Urbanos, F. A.; Puranik, V. G.; Jimenez- Aparicio, R.; Lahiri, G. K. *Inorg. Chem.* **2004**, *43*, 4911.
(7) Maurer, J.; Winter, R. F.; Sarkar, B.; Zalis, S. *J. Solid State Electrochem.* **2005**, *9*, 738.
(8) Fabrizi de Biani, F.; Dei, A.; Sangregorio, C.; Sorace, L. *Dalton Trans.* **2005**, 3868.
(9) Newell, M.; D., I. J.; Easun, T. L.; Vickers, S. J.; Adams, H. *Inorg. Chem.* **2006**, *45*, 821.

10.1021/ic060816m CCC: $37.00
Published on Web 12/16/2006

Table 1. Analysis of the Bands with a Transition Moment Larger than 0.01 Calculated with CAS1[a]

	ΔE (cm^{-1})				f_{osc}	C_x	C_y	C_z	
	CASSCF	SS-CASPT2	MS-CASPT2	SO-RASSI	D^2·μ_B	D^2·μ_B	D^2·μ_B	D^2·μ_B	nature
12^2A_u	72 500	41 900	41 800	41 800	10^{-5}	10^{-2}	-10^{-3}	10^{-4}	$\pi \rightarrow \pi^*$
11^2A_u	46 000	41 300	41 600	41 600	10^{-2}	10^{-2}	10^{-5}	-10^{-3}	$\pi \rightarrow \pi^*$
14^2B_u	72 100	41 300	41 100	41 100	10^{-3}	-10^{-5}	-10^{-2}	-10^{-5}	$\pi \rightarrow \pi^*$
13^2B_u	40 300	37 400	40 700	40 700	10^{-2}	-10^{-3}	-10^{-3}	-10^{-7}	$\pi \rightarrow \pi^*$
12^2B_u	55 200	42 700	40 600	40 500	0.1	-10^{-2}	10^{-2}	10^{-5}	$\pi \rightarrow \pi^*$
7^2B_u	38 900	16 700	24 500	24 300	10^{-3}	10^{-6}	10^{-1}	10^{-7}	$d \rightarrow \pi^{*b}$
6^2B_u	36 200	14 400	20 800	20 800	0.6	-10^{-3}	-10^{-1}	-10^{-6}	$d \rightarrow \pi^{*c}$
2^2A_u	9300	12 600	15 700	15 600	10^{-7}	-10^{-4}	10^{-2}	10^{-5}	$d \rightarrow \pi^*$
3^2B_u	8900	12 100	15 300	15 200	10^{-3}	10^{-5}	10^{-2}	-10^{-5}	$d \rightarrow \pi^*$
2^2B_u	4900	6700	6300	6400	0.1	-10^{-3}	-10^{-1}	10^{-6}	IV $\|xz\rangle$
1^2A_u	4000	4400	2800	3700	10^{-8}	10^{-2}	-10^{-1}	10^{-4}	$\|yz\rangle$
1^2B_u	3800	4100	2600	2600	10^{-4}	10^{-2}	-10^{-1}	10^{-2}	$\|x^2 - y^2\rangle$

[a] δE is the energy of the state compared to the ground state. f_{osc} is the oscillator strength and C_x, C_y, and C_z MCD transition moments. States are labeled with the spin-free symmetry and shortly described either by the localization of the hole in a d orbital or by the nature of transition. IV is the intervalence state. [b] Coupled with 2^2B_u. [c] Coupled with 1^2B_u.

Table 2. Comparison of Experiment and Theory

experiment			ΔE (cm^{-1})			CASPT2[d]			
ΔE (cm^{-1})		ϵ_{max} (M^{-1} cm^{-1})	HFS-DVM[a]	INDO[b]	DFT[c]	ΔE (cm^{-1})	f_{osc}	C_y	assignment
39 700	OA[e]	5.6×10^3	42 800	39 400	36 100	40 500	0.1		$\pi \rightarrow \pi^*$
37 000	OA[e]	shoulder	40 400	33 900		40 700	10^{-2}		$\pi \rightarrow \pi^*$
20 400	MCD[f]		21 200			24 300		10^{-1}	$\pi \rightarrow \pi^*$
17 700	OA[e]	2.1×10^4	19 000	21 100	17 600	20 800	0.6		d $\rightarrow \pi^*$
17 400	MCD[f]			20 500		20 800		-10^{-1}	d $\rightarrow \pi^*$
12 800	MCD[f]	strong pos		16 300−18 200		15 600		10^{-2}	d $\rightarrow \pi^*$
12 000	OA[e]	shoulder		9600		15 200	10^{-3}		d $\rightarrow \pi^*$
6370	OA[e]	5.5×10^3 *yz*	6600	4900	6800	6400	0.1		MC
6340	MCD[f]	weak pos *xy*[g]	6600	4900	6800	6400		-10^{-1}	MC
3200	MCD[h]	strong neg	2900	6200		3600		-10^{-1}	MC
2000	MCD[h]		2260	5900		2600		-10^{-1}	MC

[a] Reference 17. Transition operator method. [b] Reference 19. INDO/S + CISD. [c] Reference 20. PW91, base standard ADF, δSCF. [d] This work. [e] Reference 54. [f] Reference 55. [g] Reference 63. [h] References 52 and 53.

absorption spectroscopies, EPR (electronic paramagnetic resonance), and DFT (density functional theory) calculations, while the analysis of the intervalence band in this type of complexes, the effect of solvent, the effect of localization, and dynamics have been the subject of recent theoretical works.[10−14] In the CT molecule, each ruthenium is in an almost octahedral environment and one metallic atom is formally in oxidation state II corresponding to a $(t_{2g})^6$ configuration while the other one is in oxidation state III corresponding to a $(t_{2g})^5$ configuration. The electronic structure of the CT ion was first analyzed by an extended Hückel calculation by Lauher in 1980.[15] Ondrechen et al.[16,17] in 1984 and 1987 then analyzed it using the Hartree−Fock Slater Xα method: they showed the strong mixing of the two occupied d orbitals localized on each site and the lowest π^* orbital of the pyrazine bridge and furthermore calculated the transition energies with the transition operator method: they assigned with good accuracy the experimental energies determined by UV and MCD (magnetic circular dichroism) spectroscopies. In 1992, Broo and Larsson calculated the two first excitation energies at the CASSCF level with two different CASs (complete active spaces) using a minimal basis set.[18] Energies are strongly dependent on the active space. In 1997, Broo and Lincoln performed semiempirical calculations with the INDO model:[19] the optimized geometry matches well the crystallographic data (the Ru−N_{pz} distance is overestimated by 0.05 Å where N_{pz} is the nitrogen atom of the pyrazine), but transition energies are less accurate than in the previous study. In 1999, Bencini et al. carried out a geometry optimization and ΔSCF calculations to evaluate the excited states using the ADF code:[20] they found a large discrepancy in the Ru−N_{pz} distance (0.2 Å) with the standard basis set for ruthenium and a very good accuracy with an optimized basis set that is more contracted. The ΔSCF calculations are quite sensitive to the choice of density functional and basis set but they reproduce well three of the experimental bands, the best result being obtained at the crystallographic geometry with the standard basis set. All the results concerning electronic transitions will be discussed in more detail when comparing our results in Section 3, Table

(10) Reimers, J. R.; Cai, Z.-L.; Hush, N. S. *Chem. Phys.* **2005**, *319*, 39.
(11) Endicott, J. F.; Chen, Y.-J.; Xie, P. *Coord. Chem. Rev.* **2005**, *249*, 343.
(12) Distefano, A. J.; Wishart, J. F.; Isied, S. S. *Coord. Chem. Rev.* **2005**, *249*, 507.
(13) Brunschwig, B. S.; Creutz, C.; Sutin, N. *Chem. Soc. Rev.* **2002**, *31*, 168.
(14) Bailey, S. E.; Zink, J. I.; Nelsen, S. *J. Am. Chem. Soc.* **2003**, *125*, 5939.
(15) Lauher, J. W. *Inorg. Chim. Acta* **1980**, *39*, 119.
(16) Ondrechen, M. J.; Ellis, D. E.; Ratner, M. A. *Chem. Phys. Lett.* **1984**, *109*, 50.
(17) Zhang, L. T.; Ondrechen, M. J. *J. Am. Chem. Soc.* **1987**, *109*, 1666.
(18) Broo, A.; Larsson, S. *J. Am. Chem. Soc.* **1992**, *161*, 363.
(19) Broo, A.; Lincoln, P. *Inorg. Chem.* **1997**, *36*, 2544.
(20) Bencini, A.; Ciofini, I.; Daul, C. A.; Ferretti, A. *J. Am. Chem. Soc.* **1999**, *121*, 11418.

2. In 2002, Marynick et al.[21] compared the MP2 (second-order Møller−Plesset) and DFT methods using the Gaussian code to describe the geometry of the CT ion. MP2 gives an accurate geometry while, whatever the basis set or the functional, (they have tried 10 basis sets and five functionals), the $Ru-N_{pz}$ distance is overestimated by 0.2 Å with DFT. Recently, Reimers et al.[10] have calculated the reorganization energy accompanying electron transfer in this molecule.

The calculation of excited states in transition metal complexes is a challenging task. The CASPT2 method is known to give satisfying results but is restricted to medium-sized molecules, whereas TD-DFT emerges as a very promising tool for the description of excited states as long as they are dominated by single excitations and there is no charge transfer. There are numerous studies of monometallic complexes of ruthenium[22−26] but rather few studies of excited states of bimetallic species except the description of the magnetic properties that requires only the first very low lying states with properties very close to the ones of the ground state. To our knowledge, the calculation of the MCD transition moments are restricted to the A and B terms.[27,28] In this article, we propose a method to calculate these transition moments. Finally, different methods for the calculation of *g*-factors from first principles are now available using DFT[29] but their application on bimetallic species[30−32] is recent. An alternative method[33] that gives good results on benchmark molecules will be applied in the present study.

In this work, we report the results of CASSCF/CASPT2 calculations of the CT ion at its crystallographic geometry. The aim of this article is the comparison of the ab initio calculations of excited states and of *g*-factors of the CT ion with experiment. In a previous article,[34] we have shown how a multi-center effective Hamiltonian can be extracted from wave function-based calculations and that such model Hamiltonians are able to reproduce the lower part of the excitation spectrum. This article validates the use of a superexchange model Hamiltonian to describe electron transfer in such molecules and analyzes the definition of the local parameters. We will furthermore show that a multi-reference description is essential even to describe correctly the ground state: two main configurations with different energies are in competition, and their energetic order is reversed after one takes into account the dynamical correlation. The consequence is that it is very difficult to describe correctly the nature of the ground state and its energy. We find that the CASSCF/CASPT2 method reproduces reasonably well all the known experimental bands and predicts the rest of the spectrum which is of an unsuspected richness, 350 states below 50 000 cm^{-1}. To assign correctly the calculated bands to the experimental ones, MCD transition moments have been calculated. Finally, *g*-factors have been evaluated, compared to the experimental values, and analyzed in terms of a model Hamiltonian. All these calculations have been done with a symmetrical geometry of the complex and with the two metallic centers being related by symmetry. This also implies that no information is provided concerning the localization or the delocalization of the electron between the two centers.

Computational details are given in Section 2 and results discussed in Section 3.

2. Computational Details

2.1. Ab Initio Calculations. All calculations have been performed using all-electron basis sets: the ruthenium is described by the basis set 7s6p4d of Faegri and Wahlgren[35] while carbon and nitrogen atoms are described by cc-pVDZ basis sets of Dunning.[36] Hydrogen atoms are described with the 3-21G basis set.[37] The effect of the basis set has been analyzed by adding a f function of exponent 1.0 on the ruthenium atom with exponent 1.0 or by using cc-pVTZ basis set on the nitrogens and carbons of the bridging ligand.

Calculations have been performed using the MOLCAS-6 program system[38] at the CASSCF[39] and CASPT2[40] levels of theory. All the states are coupled after calculation of perturbation following the multi-state-CASPT2 (MS-CASPT2) scheme,[41] and a real level shift of 0.5 is used.[42] Scalar relativistic effects are taken into account by means of of the Douglas−Kroll−Hess transformation,[43] and spin−orbit coupling is calculated with the SO-RASSI[44] code using the AMFI approximation for the calculation of the spin−orbit integrals.[45] Two active spaces have been used; CAS1 consists of 15 electrons in 10 MOs, the two highest π and the two lowest π^* orbitals of the pyrazine, and the six t_{2g}-like orbitals of the ruthenium atoms (see Figure 2). CAS2 consists of 11 electrons in 12 MOs, the two lowest π^* orbitals of the pyrazine and the 10 d orbitals of the metallic atoms. State-averaged CASSCF calculations have been

(21) Hardesty, J.; Goh, S. K.; Marynick, D. S. *J. Mol. Struc. THEOCHEM* **2002**, *588*, 223.
(22) Wang, F.; Ziegler, T. *J. Chem. Phys.* **2005**, *123*, 194102.
(23) Batista, E. R.; Martin, R. L. *J. Phys. Chem. A* **2005**, *109*, 3128.
(24) Charlot, M. F.; Pellegrin, Y.; Quaranta, A.; Leibl, W.; Aukauloo, A. *Chem. Eur. J.* **2006**, *12*, 796.
(25) Fantacci, S.; De Angelis, F.; Wang, J.; Bernhard, S.; Selloni, A. *J. Am. Chem. Soc.* **2004**, *126*, 9715.
(26) De Angelis, F.; Fantacci, S.; Sgamelotti, A.; Cariati, F.; D., R.; Tessore, F.; Ugo, R. *Dalton Trans.* **2006**, 852.
(27) Coriani, S.; Jørgensen, P.; Rizzo, A.; Ruud, K.; Olsen, J. *Chem. Phys. Lett.* **1999**, *300*, 61.
(28) Honda, Y.; Hada, M.; Ehara, M.; Nakatsuji, H.; Michl, J. *J. Chem. Phys.* **2005**, *123*, 164113.
(29) Kaupp, M., Bühl, M., Malkin, G., Eds. *Calculation of NMR and EPR parameters*; WILEY-VCH: Weinheim, 2004.
(30) Sinnecker, S.; Neese, F.; Noodleman, L.; Lubitz, W. *J. Am. Chem. Soc.* **2004**, *126*, 2613.
(31) Sinnecker, S.; Neese, F.; Noodleman, L.; Lubitz, W. *J. Biol. Inorg. Chem.* **2005**, *10*, 231.
(32) Kababya, S.; Nelson, J.; Calle, C. Neese, F.; Goldfarb, D. *J. Am. Chem. Soc.* **2006**, *128*, 2017.
(33) Bolvin, H. *ChemPhysChem* **2006**, *7*, 1575.
(34) Bolvin, H. *J. Phys. Chem. A* **2003**, *107*, 5071.
(35) Wahlgren, U.; Faegri, K. *MOLCAS Library*.
(36) Dunning, T. H. J. *J. Chem. Phys.* **1989**, *90*, 1007.
(37) Binkley, J. S.; Pople, J. A.; Hehre, W. J. *J. Am. Chem. Soc.* **1980**, *102*, 939.
(38) Karlström, G.; Lindh, R.; Malmqvist, P.-A.; Roos, B. O.; Ryde, U.; Veryazov, V.; Widmark, P.-O.; Cossi, M.; Schimmelpfennig, B.; Neogrady, P.; Seijo, L. *Comput. Mater. Sci.* **2003**, *28*, 222.
(39) Roos, B. O.; Taylor, P. R.; Siegbahn, P. E. M. *Chem. Phys.* **1980**, *48*, 157.
(40) Andersson, K.; Malmqvist, P.-A.; Roos, B. O.; Sadlej, A. J.; Wolinski, K. *J. Phys. Chem.* **1990**, *94*, 5483.
(41) Finley, J.; Malmqvist, P.-A.; Roos, B. O.; Serrano-Andres, L. *Chem. Phys. Lett.* **1998**, *288*, 299.
(42) Roos, B. O.; Andersson, K. *Chem. Phys. Lett.* **1995**, *245*, 215.
(43) Hess, B. A. *Phys. Rev. A* **1986**, *33*, 3742.
(44) Malmqvist, P.-A.; Roos, B. O.; Schimmelpfennig, B. *Chem. Phys. Lett.* **2002**, *357*, 230.
(45) Hess, B. A.; Marian, C. M.; Wahlgren, U.; Gropen, O. *Chem. Phys. Lett.* **1996**, *96*, 365.

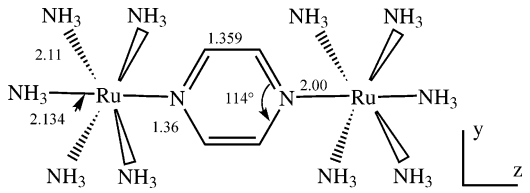

Figure 1. Scheme of the CT ion with geometrical parameters used in the calculations. Distances are in Å.

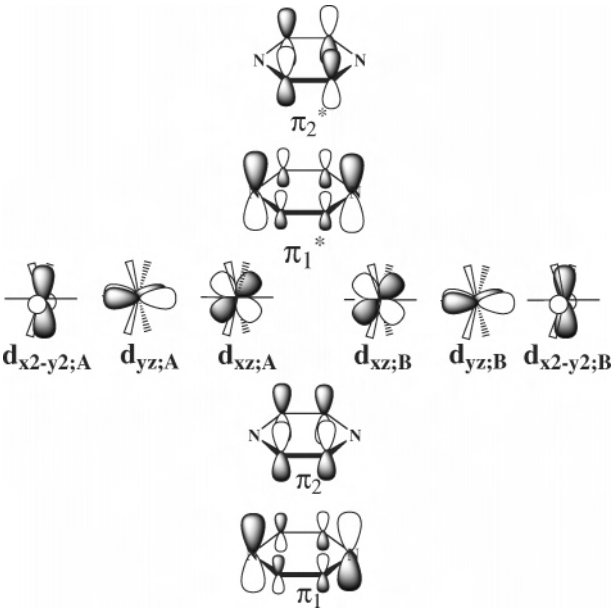

Figure 2. Schematic view of the active orbitals.

performed with, for CAS1, 28 roots for doublet states and 16 for quartet states and, for CAS2, 70 roots for the doublet states and 55 roots for the quartet states. This large number of roots is necessary to get the right description of the ground state; the configurations with one hole in the t_{2g}-like orbitals are high in energy, about 40 000 cm^{-1} above the ground state at the SCF level, and then there are many roots below them. Transition dipole and angular moments are calculated with the RASSI program[46] using the vectors obtained in the MS-CASPT2 calculation. In one of the calculations, solvent effects have been added using a polarizable continuum model (PCM) model[47] with the parameters for water. Nonequilibrium solvation has been used for the calculation of excited states.[48]

Calculations are performed on the CT ion, $[(NH_3)_5-Ru-pyrazine-Ru-(NH_3)_5]^{5+}$, slightly idealized compared to the crystallographic data:[49,50] the aromatic cycle is planar, all the bonds around the ruthenium atoms are perpendicular to each other, and the distances are summarized in Figure 1. Ammonium molecules are rotated in such a way that the molecule belongs to the C_{2h} group. The intermetallic axis is the *z* axis, and the pyrazine ring lies in the *yz* plane. The atoms of the monomer $[(NH_3)_5-Ru-pyrazine]^{3+}$ have been kept in their positions in the dimer; this molecule belongs to the C_s point group.

2.2. Magnetic Circular Dichroism Transition Moments. The contribution of the $0 \rightarrow f$ transition to the *C* term in direction *u* (*u* = *x*, *y*, *z*) is calculated using eq 21 of the Appendix

$$C_u(0f) = -3\mu_B g_e S_u(\Phi_0{}^u\Phi_0{}^u)[\mathrm{Im}\{\vec{\mu}(\Phi_0^u\Phi_f^u)\} \wedge \mathrm{Re}\{\vec{\mu}(\Phi_0^u\Phi_f^u)\} - \mathrm{Im}\{\vec{\mu}(\Phi_0^u\overline{\Phi_f^u})\} \wedge \mathrm{Re}\{\vec{\mu}(\Phi_0^u\overline{\Phi_f^u})\}]_u \quad (1)$$

where $S_u(\Phi_I\Phi_J) = \langle\Phi_I|\hat{S}_u|\Phi_J\rangle$, $\vec{\mu}(\Phi_I\Phi_J) = \langle\Phi_I|\vec{\mu}|\Phi_J\rangle$, $\hat{S}_u$ is the projection on *u* axis of the total spin angular momentum operator, $\vec{\mu}$ is the electric dipole operator, μ_B the Bohr magneton, g_e, the Landé factor of the free electron, Φ_i^u and $\overline{\Phi_i^u}$ are the Kramers partners of the *i*-th state with quantization axis *u*, and Re and Im denote that the real and imaginary parts of the quantity within parentheses are to be used, respectively. Φ_i^z and $\overline{\Phi_i^z}$ with $i = 0$ or *f* are calculated by the SO-RASSI program with MS-CASPT2 vectors, Φ_i^x, Φ_i^y, $\overline{\Phi_i^x}$ and $\overline{\Phi_i^y}$ are deduced using eqs 19 and 20, and transition dipole moments $\vec{\mu}(\Phi_0^u\Phi_f^u)$ are calculated by the RASSI program.

2.3. *g*-Factors. *g*-Factors have been determined from first principles following the method described in a recent publication .[33] The Zeeman interaction δE is described by the Zeeman Hamiltonian

$$\hat{\mathscr{H}}_{ZE} = \mu_B(\vec{L} + g_e\vec{S})\cdot\vec{B} = -\vec{m}\cdot\vec{B} \quad (2)$$

where $\vec{B}$ is the applied magnetic field, μ_B is the Bohr magneton, g_e is the Landé factor of the free electron, and $\vec{m}$ is the magnetic moment. This interaction is modeled by a spin Hamiltonian

$$\hat{\mathscr{H}}_S = \mu_B\vec{B}\cdot\mathbf{g}\cdot\tilde{S} \quad (3)$$

where **g** is the electronic *g*-matrix and $\tilde{S}$ is a pseudo-spin vector. Matrix elements of **g** are chosen to reproduce the eigenvalues of eq 2 and are given by

$$\mathbf{g} = \mathbf{\Lambda} + g_e\mathbf{\Sigma} \quad (4)$$

where the matrices $\mathbf{\Lambda}$ and $\mathbf{\Sigma}$ are defined by

$$\Omega_{ux} = 2\mathrm{Re}(\langle\overline{\Phi_0^z}|\hat{O}_u|\Phi_0^z\rangle) = 2\mathrm{Re}(\langle\Phi_0^z|\hat{O}_u|\overline{\Phi_0^z}\rangle)$$

$$\Omega_{uy} = 2\mathrm{Im}(\langle\overline{\Phi_0^z}|\hat{O}_u|\Phi_0^z\rangle) = -2\mathrm{Im}(\langle\Phi_0^z|\hat{O}_u|\overline{\Phi_0^z}\rangle)$$

$$\Omega_{uz} = 2(\langle\Phi_0^z|\hat{O}_u|\Phi_0^z\rangle) = -2\langle\overline{\Phi_0^z}|\hat{O}_u|\overline{\Phi_0^z}\rangle \quad (5)$$

for $u = x, y, z$ and $(\Omega, \vec{O}) = (\Lambda, \vec{L})$ or $(\Sigma, \vec{S})$. These equations have the same form as eqs 22 and 23, p 135 of ref 51 where they were derived in the specific case of $u = z$, a monoelectronic wave function and a monocentric spin−orbit operator. Using eqs 19 and 20 of the Appendix, eqs 5 can be written more compactly as

$$\Omega_{uv} = 2(\langle\Phi_0^v|\hat{O}_u|\Phi_0^v\rangle) = -2\langle\overline{\Phi_0^v}|\hat{O}_u|\overline{\Phi_0^v}\rangle$$

with $u,v = x, y, z$. As for MCD transition moments, Φ_0^z and $\overline{\Phi_0^z}$ are determined by the MS-CASPT2 + SO-RASSI method. Transition angular moments are evaluated using RASSI program taking the center of charges of the nuclei as the origin. This method gives good results on benchmark molecules in comparison to experimental

(46) Malmqvist, P.-A. *Int. J. Quantum Chem.* **1986**, *30*, 479.
(47) Miertus, S.; Scrocco, E.; Tomasi, J. *Chem. Phys.* **1981**, *55*, 117.
(48) Cossi, M.; Barone, V. *J. Chem. Phys.* **2001**, *115*, 4708.
(49) Beattie, J. K.; Hush, N. S.; Taylor, P. R.; Raston, C. L.; White, A. H. *Chem. Soc., Dalton Trans.* **1977**, 1121.
(50) Fürholz, U.; Bürgi, H.; Wagner, F. E.; Stebler, A.; Ammeter, J. H.; Krausz, E.; Clark, R. J. H.; Stead, M. J.; Ludi, A. *Chem. Soc., Dalton Trans.* **1977**, 1121.
(51) Carrington, A.; McLachlan, A. D. *Introduction to magnetic resonance*; Harper and Row: London, 1967.

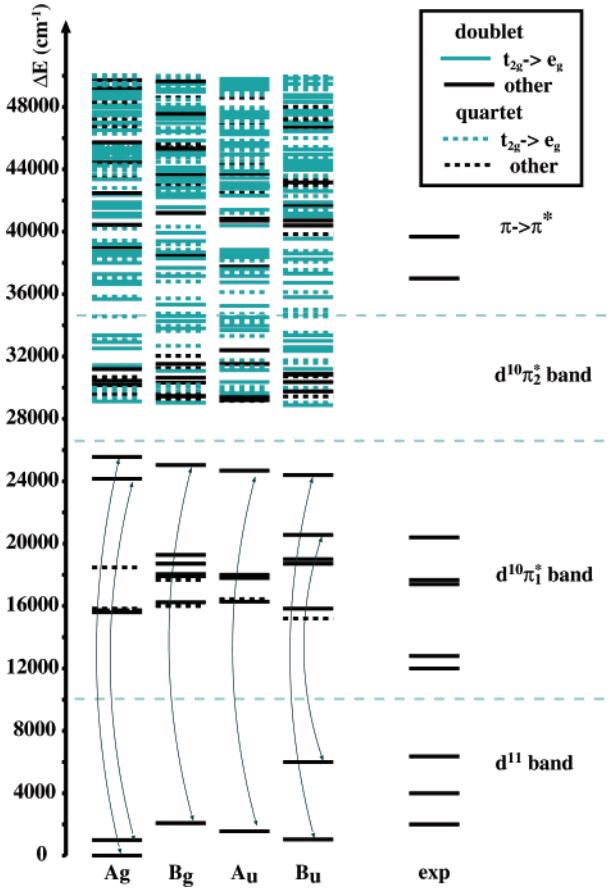

Figure 3. Energy levels in cm^{-1} of the CT ion calculated at the MS-CASPT2 level. The reference of the energies is the ground state (^2Ag). The arrows represent the couplings.

values and previous studies and is completly adapted to this study because all the excited states have already been calculated.

3. Results and Discussion

3.1. Spectrum of the Excited States. Energies of the excited states relative to the ground state are represented in Figure 3. They are calculated at the MS-CASPT2 level and are classified according to their irrep. There are about 350 states below 50 000 cm^{-1} that can be analyzed the following way:

(i) The six first ones with a hole in one of the six t_{2g}-like orbitals, they are ligand-field (LF) states. As has been discussed already in reference 34, the nature of these states depends strongly on dynamical correlation through the mixing of two configurations, the first one with one hole in the t_{2g}-like orbitals denoted d^{11} and the second one, denoted $d^{10}\pi^*$, with one excitation from a d orbital to the first π^* orbital, π_1^*. At the MS-CASPT2 level, the weight on the first configuration is 0.69 while it is 0.36 before correlation. The ground state corresponds to one hole in the gerade combination of d_{xz} orbitals and is of ^2A_g symmetry before introduction of spin−orbit coupling. The next states have a hole in combinations of $d_{x^2-y^2}$ or d_{yz} orbitals, the two other t_{2g}-like orbitals. Finally, the last state of this band is a ^2B_u state with a hole in the ungerade combination of d_{xz} orbitals; this state is destabilized compared to the previous ones due to the large π overlap of the ungerade combination of d_{xz} with the π_1^* orbital: it is the intervalence state, its energy compared to the ground state is usually denoted $2V_{AB}$, twice the effective coupling between the metallic centers that characterizes the electronic delocalization between the centers.

(ii) The next band consists of states with one electron in the π_1^* orbital; they are metal-to-ligand charge transfer (MLCT) states. There are 25 such states, either doublet or quartet states. Six of them are strongly destabilized compared to the other states of this band due to their interaction with the states of the first band; these six states are developped on the same determinants as states of the first band. This band lies in the range 15 000−25 000 cm^{-1}.

(iii) From 28 000 cm^{-1}, there is a large number of states with excitation in a e_g-like orbital, there are metal-centered (MC) transition states. This band is by far the most dense one.

(iv) Overlapping the previous one, another band consists of states with one electron in the π_2^*, these are MLCT states again. There are 25 such states, either doublet or quartet states. This band lies in the range 28 000−32 000 cm^{-1}.

(v) Finally, overlapping again the MC band, from 30 000 cm^{-1}, the states corresponding to an excitation from a π to a π^* orbital, they are ligand-centered (LC) transitions.

The main conclusion of the analysis of this spectrum is that there is a quasi continuum of states from 28 000 cm^{-1}: it is due to the fact that the ground state has open shells within almost degenerate orbitals and that there are quasi degenerate low lying vacant orbitals of different type: e_g-like and π^* orbitals.

In order to compare the theoretical spectrum to the experimental bands, transition moments have been calculated. As shown in Section 2.2, it is necessary to include spin−orbit interaction to obtain the MCD transition moments since the ground state is orbitally non-degenerate. Transitions with MCD moments larger than 0.01 $D^2 \cdot \mu_B$ or optical transitions with an oscillator strength larger than 0.01 have been selected and are analyzed in more detail in Table 1. The introduction of dynamical correlation has important consequences, especially on states with d^{11} configuration because they have one more doubly occupied d orbital than the other ones. Let us focus on the 1^2B_u and 6^2B_u states as an example: at the CASSCF and SS-CASPT2 (single-state CASPT2) levels 1^2B_u can be written $c_1|d^{11}\rangle + c_2|d^{10}\pi^*\rangle$ and 6^2B_u as $c_2|d^{11}\rangle - c_1|d^{10}\pi^*\rangle$ with $c_1 < c_2$. The energy gap is reduced after introduction of dynamical correlation and the two states mix together in the MS-CASPT2 step so that 1^2B_u becomes mainly a d^{11} configuration and 6^2B_u a $d^{10}\pi^*$ one ($c_1 > c_2$). The influence of dynamical correlation is very important on some $\pi \rightarrow \pi^*$ transitions as well. The MS-CASPT2 step is thus crucial for the first six states and especially for the ground state: the coupling matrix element that couples the two states with configurations d^{11} and $d^{10}\pi^*$ determine the respective weights of these configurations in the ground state and its energy: an overestimation of this element will overestimate the weight of the d^{11} configuration in the ground state and its energetic stabilization. It is the case with CAS2

where the ground state becomes by far too low by MS-CASPT2 coupling. Results with CAS1 are more reliable. The introduction of spin−orbit coupling has only small consequences. Except for the three first states and their coupled states, all the states that have large transition moments with the ground state have an important spin density on d_{xz} orbitals. It means that between the forest of states that correspond to a d → π^* or $\pi \rightarrow \pi^*$ transitions, one detects the ones with a hole in this latter d orbital and with a coupling of the local spins that gives a nonzero spin density in this orbital.

These calculated bands are compared in Table 2 to experimental bands and previous calculations using Xα,[17] semiempirical INDO,[18] or DFT[20] methods. The assignment of the three first bands agrees with Xα and INDO methods: they correspond to LF transitions between the t_{2g}-like orbitals, the last one at 6370 cm^{-1} being the IV transition. The calculated oscillator strength of the IV transition is large. These three bands are detected by MCD,[52,53] the second one giving rise to a large negative signal while the IV band gives rise to a weak positive signal: the sign of the calculated moment is right for the former but not for the latter. In the range 12 000−25 000 cm^{-1}, all the bands are assigned to MLCT, d → π^*, transitions. The shoulder in the optical spectrum at 12 000 cm^{-1} [54] can be assigned to the weakly absorbing calculated band at 15 200 cm^{-1} and was previously only assigned with INDO calculations. The strong positive signal in the MCD spectrum at 12 800 cm^{-1} [55] corresponds to the calculated band with large positive MCD moment at 15 600 cm^{-1} and has never been assigned by calculations before. The sign of the next band at 17 400 cm^{-1} is not given in the publication. The calculated band at 20 800 cm^{-1} has both large oscillator strength and negative MCD moments; thus, we assign it to the MCD band at 17 400 cm^{-1} and to the optical band at 17 700 cm^{-1}. The bands calculated at 20 800 and 24 300 cm^{-1} have a non-negligible weight on the d^{11} configuration because of the coupling with the LF states. The three last observed bands correspond to $\pi \rightarrow \pi^*$ transitions, according to our calculations. For the first one at 20 400 cm^{-1} detected with MCD, one finds a large positive MCD moment; the sign of this transition was not given in the publication. This band was assigned to LF transition with Xα calculations and was not found with other methods. The optical band at 39 700 cm^{-1} shows a large calculated oscillator strength. It had been found by all previous methods and assigned to the same type of transition. The shoulder in the optical spectrum at 37 000 cm^{-1} can be assigned to the calculated band at 40 700 cm^{-1} because of its oscillator strength, but there is a reversal in the energetic order. This band was assigned to a LMCT transition by Xα calculations and not assigned by other methods. All optical transitions are polarized along the *z* axis, while all MCD transitions are polarized along the *y* axis.

Table 3. Transition Energies in cm^{-1} in the Monomer and the Dimer

	monomer		dimer	
hole	sym	energy	sym	energy
d_{xz}	$^2A'$	0	^2A_g	0
			^2B_u	6400
$d_{x^2-y^2}$	$^2A'$	2200	^2A_g	2400
			^2B_u	2600
d_{yz}	$^2A''$	3300	^2A_u	3400
			^2B_g	2800

Except the LF bands and the last $\pi \rightarrow \pi^*$ transition, all excitation energies are overestimated by about 3000 cm^{-1}. It means that the six LF states are too low in energy and that the coupling between the two configurations by MS-CASPT2 is overestimated. It appears that the whole spectrum of Figure 3 should be translated by about 3000 cm^{-1} downwards, except the bands below 10 000 cm^{-1}, and that the MS-CASPT2 calculation overestimates the weight on the d^{11} configuration; its weight should be less than 0.69. The effect of the basis set has been checked on the model molecule $[NCH-(NH_3)_4-Ru-pyrazine-Ru-(NH_3)_4NCH]^{5+}$. Adding a polarization f function on the ruthenium atoms reduces the gap between the two configurations $d^{10}\pi^*$ at the SS-CASPT2 level by 4000 cm^{-1} because it allows a better description of the dynamical correlation in the d^{11} configuration and finally enhances the coupling between the two configurations at the MS-CASPT2 step putting the d^{11} configuration block 2500 cm^{-1} downward. At the opposite, a better description of the atoms of the bridge with a cc-pVTZ basis gives a larger gap between the two configurations by 1000 cm^{-1} and reduces the coupling by 1000 cm^{-1}. The conclusion is that the MS-CASPT2 step is qualitatively correct because it rectifies the nature of the ground state but is quantitatively wrong and depends strongly on both active space and basis set.

The effect of solvation has been analyzed on the same model molecule: there is strictly no effect on the composition of the wave function and on the MS-CASPT2 coupling and the effect is less than 500 cm^{-1} on energy gaps. This clearly shows that the effect of solvation is negligible as long as the molecule is kept symmetrical.

Let us now analyze the LF states to get more insight into the MOs of the complex and to be able to propose a model Hamiltonian for the next section. It is fruitful to compare the LF states of the dimer with those of the monomer $[(NH_3)_5-Ru-pyrazine]^{3+}$, see Table 3. All the states are very similar in the two compounds except for the ungerade combination $|xz_u\rangle$ of the $|xz\rangle$ states with a hole in the d_{xz} orbitals. The ligand field slightly splits the d_{yz} and $d_{x^2-y^2}$ orbitals, giving rise to a rhombic distortion of energy *E*. The main effect of the π system is due to the π_1 and π_1^* orbitals shown on Figure 2 which have significant coefficients on the nitrogen atoms. Both π_1 and π_1^* can interact with the d_{xz} orbital in the monomer, while π_1 can only interact with the gerade combination d_{xz}^g of the d_{xz} and π_1^* orbitals with the ungerade d_{xz}^u combination of the d_{xz} orbitals due to symmetry. For the monomer, the energies of the LF states and the canonical MOs show that the interaction with π_1 orbital is predominant and the MO diagram of Figure 4 can be

(52) Krausz, E. R. *Chem. Phys. Lett.* **1985**, *120*, 113.
(53) Krausz, E. R.; Mau, A. W. H. *Inorg. Chem.* **1986**, *25*, 1484.
(54) Creutz, C.; Taube, H. J. *J. Am. Chem. Soc.* **1973**, *95*, 1073.
(55) Krausz, E. R.; Ludi, A. *Inorg. Chem.* **1985**, *24*, 939.

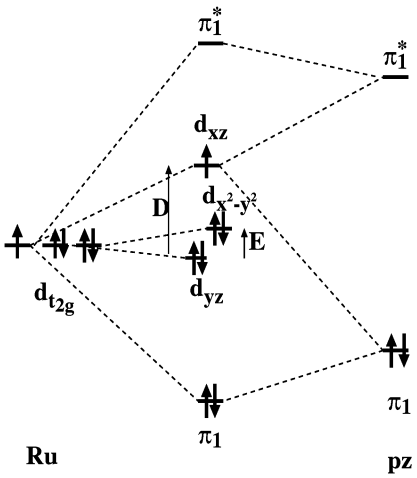

Figure 4. Schematic scheme of the MOs of the monomer.

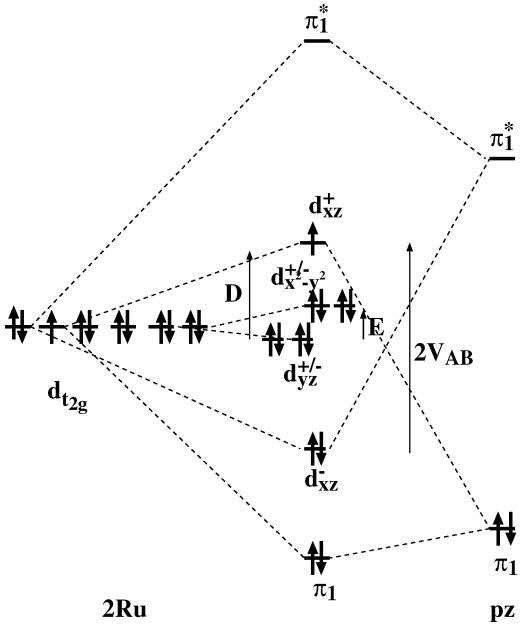

Figure 5. Schematic scheme of the MOs of the dimer.

proposed: this destabilization of the d_{xz} orbital corresponds to the axial distortion of energy *D*. For the dimer, the energies of the LF states show that there is a large stabilization of d^u_{xz} orbitals by interaction with π_1^* orbital. The MO diagram for the dimer is proposed in Figure 5: this interaction with the π_1^* orbital is specific to the dimer and gives rise to the splitting of the d^g_{xz} and d^u_{xz} orbitals by an energy of $2V_{AB}$.

To conclude, the ground state is strongly multiconfigurational and must be described by a noncontracted method to let the respective weights of the configurations be corrected after the inclusion of correlation. For the first time, all the experimental bands have been assigned and our calculations suggest that all the three highest experimental bands are $\pi \rightarrow \pi^*$ transitions, contrary to previous assignments. Due to the large density of states, the assignment of the observed bands was only possible by calculating the transition moments. It is, to our knowledge, a first attempt to calculate C term MCD transition moments from first principles. For each observed band, one finds in the same region of energy a level with a MCD moment larger than 0.01 $D^2 \cdot \mu_B$, the sign is correct for two of the bands among the three for which the sign is known. There is a systematic error of 3000 cm^{-1} for the non-LF states because of an overestimation of the coupling in the MS-CASPT2 step. We have shown the richness of the spectrum that is almost a continuum from 28 000 cm^{-1} and that the π_1 orbital of the pyrazine is the main factor of the axial distortion of the ligand field while the π_1^* orbital plays the key role of the coupling between the two metallic sites.

3.2. *g*-Factors. The calculated principal axes are almost (within 99.94%) the molecular ones. After diagonalization, one finds (the notation will neglect the rotation of the axis) $g_x = 1.54$, $g_y = 2.76$, and $g_z = 2.47$ for CAS1 and $g_x = 1.59$, $g_y = 2.70$, and $g_z = 2.52$ for CAS2. Experimental values are $g_x = 1.334$, $g_y = 2.779$, and $g_z = 2.489$ according to Hush et al.[56] and $g_x = 1.346$, $g_y = 2.799$, and $g_z = 2.487$ according to Stebler et al.[57] The values in the *y* and *z* directions are well reproduced by our calculations, but it is not the case in the *x* direction, the results being only qualitatively correct in this direction. Results obtained with CAS1 are better than the ones with CAS2. The analysis per state introduced in ref 33 shows that there is no contribution from the quartet states and that the main contributions come from the two first excited states of symmetry A_g and B_g, namely the states with a hole in a t_{2g}-like orbital. It confirms the choice of the two previous publications to limit the model space to those states; they can be written as monoelectronic functions characterized by the localization of the lone electron or equivalently of the hole. The basis set is formed by the 12 states $|xz_{A/B}; \alpha/\beta\rangle$, $|x^2 - y^2_{A/B}; \alpha/\beta\rangle$ $|yz_{A/B}; \alpha/\beta\rangle$ where $|xz_A;\alpha\rangle$ means that the lone electron is localized in the d_{xz} orbital of Ru_A with a spin up and so on for the other ones. A delocalized basis set can be used too with

$$|d_{\pm}; \sigma\rangle = \frac{1}{\sqrt{2}}(|d_A; \sigma\rangle \pm |d_B; \sigma\rangle) \tag{6}$$

$d = xz$, $x^2 - y^2$, yz and $\sigma = \alpha$, β. The model Hamiltonian takes the form

$$\hat{\mathcal{H}} = \hat{\mathcal{H}}_{\mathcal{A}} + \hat{\mathcal{H}}_{\mathcal{B}} + \hat{\mathcal{H}}_{\mathcal{AB}} \tag{7}$$

$\hat{\mathcal{H}}_I$ (I = A,B) is a one-center term

$$\hat{\mathcal{H}}_I = -\frac{D}{3}\left\{\hat{L}^2_{yI} - \frac{1}{3}L(L+1)\right\} + \frac{E}{6}\{\hat{L}^2_{xI} - \hat{L}^2_{zI}\} + \lambda \vec{L}_I \cdot \vec{S}_I \tag{8}$$

The two first terms describe the deformation from octahedral environment where *D* and *E* are the axial and rhombic ligand field parameters as discussed in the previous section and the third term modelizes spin−orbit coupling. This one-center Hamiltonian is the same as in the publication of Stebler et al.[57] neglecting the effect of the orbital reduction parameter while Hush et al.[56] had omitted the rhombic term. $\hat{H}_{AB}$ models the interaction between sites A and B

(56) Hush, N. S.; Edgar, A.; Beattie, J. K. *Chem. Phys. Lett.* **1980**, *69*, 128.
(57) Stebler, A.; Ammeter, J. H.; Fürholz, U.; Ludi, A. *Inorg. Chem.* **1984**, *23*, 2764.

$$\hat{\mathcal{H}}_{AB} = 2V_{AB}\{|xz_-;\alpha\rangle\langle xz_-;\alpha| + |xz_-;\beta\rangle\langle xz_-;\beta|\}$$

Only the ungerade combination of the d_{xz} orbitals is perturbed by the coupling between the two centers as discussed previously. V_{AB} is the electronic effective coupling parameter between the two sites discussed extensively in a previous publication .[34] This model is very close to the one proposed by Ko et al.[17,58] except that the role of symmetry was not discussed; in the model Hamiltonian, the coupling seems to concern the symmetric combination of d_{xz} orbitals, in the expression of energies, it concerns the antisymmetric combination and *g*-factors depends on the electronic coupling while it should not. Furthermore, we have shown that there is no need to introduce a MLCT state. One finds that

$$\langle d_\pm;\sigma|\hat{\mathcal{H}}|d'_\pm;\sigma'\rangle = \langle d_A;\sigma|\hat{\mathcal{H}}_{\mathcal{A}}|d'_A;\sigma'\rangle + \langle d_A;\sigma|\hat{\mathcal{H}}_{\mathcal{AB}}|d'_B;\sigma'\rangle$$

and evidently

$$\langle d_\pm;\sigma|\hat{\mathcal{H}}|d'_\mp;\sigma'\rangle = 0 \tag{9}$$

with d, d′ = xz, $x^2 - y^2$, yz and σ, $\sigma' = \alpha$, β. The matrix of Hamiltonian of eq 8 in the basis of eq 6 gives rise to four block-submatrices of dimension 3, two sets of two equivalent matrices describing the interaction between the symmetrical and unsymmetrical states that are decoupled by eq 9. Consequently, to find the ground state, one has only to diagonalize the following matrix

$$\begin{bmatrix} |xz_+;\alpha\rangle & |x^2-y^2_+;\beta\rangle & |yz_+;\alpha\rangle \\ -\frac{2}{3}D & -\frac{1}{2}\lambda & \frac{i}{2}\lambda \\ -\frac{1}{2}\lambda & \frac{1}{3}D-\frac{1}{2}E & -\frac{i}{2}\lambda \\ -\frac{i}{2}\lambda & \frac{i}{2}\lambda & \frac{1}{3}D+\frac{1}{2}E \end{bmatrix} \tag{10}$$

In the case of shells more than half filled, λ is negative, and supposing $D > E/2 > 0$, the solution for the ground state has the form

$$|\Psi_0\rangle = a|xz_+;\alpha\rangle - b|x^2-y^2_+;\beta\rangle + ic|yz_+;\alpha\rangle$$

$$|\bar{\Psi}_0\rangle = a|xz_+;\beta\rangle + b|x^2-y^2_+;\alpha\rangle - ic|yz_+;\beta\rangle \tag{11}$$

Applying eq 4 one finds the expression for the *g*-factors

$$g_{xx} = g_e - 2(b^2+c^2)g_e - 4bc$$

$$g_{yy} = g_e - 2c^2 g_e + 4ab$$

$$g_{zz} = g_e - 2b^2 g_e + 4ac \tag{12}$$

the same equations as in ref 57 and p 280 of ref 59. With such a model, the matrix of eq 10 is independent of the coupling factor V_{AB} because the ground state is gerade while the coupling only affects an ungerade state; *g*-factors are therefore independent of V_{AB} as well. *D*, *E*, and λ are one-center parameters, so *g*-factors should be the same in the monomer as in the dimer. This is indeed confirmed by our calculations (see Tables 3 and 4). This is contrary to the conclusions by Ondrachen et al.[58] *D*, *E*, and V_{AB} can be deduced from the calculations before spin−orbit coupling: $D = 2800\ cm^{-1}$, $E = 800\ cm^{-1}$, and $V_{AB} = 3200\ cm^{-1}$ seem to be reasonable values given the different states of Table 3 and are in good agreement with those deduced by Stebler. From SO-RASSI calculations, one then gets $a = 0.960$, $b = 0.224$, and $c = 0.169$; with these values, eqs 5 and 12 give $\Sigma_{xx} = 0.84$, $\Lambda_{xx} = -0.15$, $g_{xx} = 1.53$, $\Sigma_{yy} = 0.94$, $\Lambda_{yy} = 0.84$, $g_{yy} = 2.72$, $\Sigma_{zz} = 0.90$, $\Lambda_{zz} = 0.65$, and $g_{zz} = 2.45$. The two largest contributions, Λ_{yy} and Λ_{zz}, are the only nonvanishing contributions considered by perturbation approaches; they are due to the interaction of the ground state with the first excited state through $\hat{L}_y$ and with the second excited state through $\hat{L}_z$, respectively. All spin contributions are negative because they correspond to the decrease of magnetic moment due to spin−orbit coupling in the considered direction. It appears that $\Delta g_x = g_{xx} - g_e$ is very different from zero because both spin and orbital contributions are negative. The latter one is due to the coupling between the two excited states through $\hat{L}_x$; even if both contributions are of second order in the spin−orbit coupling perturbation, namely in parameters *b* and *c*, the anisotropy in this direction is of the same order of magnitude as in the two other directions. It is the direction with the largest discrepancy in the calculation of the *g*-factor: it seems to confirm the conclusion of our previous study[33] that second-order contributions are more difficult to calculate. Finally, as done by Stebler, parameters can be extracted by fitting the *g*-values: there are only two independent parameters to describe eigenvectors of matrix of eq 10: $\epsilon_1 = (D - E/2)/(-\lambda)$ and $\epsilon_2 = (D + E/2)/(-\lambda)$. To fit the *g*-values calculated with ab initio methods, one gets $\epsilon_1 = 2.31$ and $\epsilon_2 = 3.28$ giving $a = 0.960$, $b = 0.224$, $c = 0.170$; it shows that the model is suitable to reproduce the full ab initio calculation with $\lambda = -1000\ cm^{-1}$. On the other hand, the fit of the experimental *g*-values gives $\epsilon_1 = 1.97$ and $\epsilon_2 = 2.71$ giving $a = 0.944$, $b = 0.259$, $c = 0.203$. In this case, *b* and *c* are greater than previously, the interaction between the ground state and the excited states is thus larger; the model of eq 7 can reproduce these values of *b* and *c* and consequently give the experimental values for the *g*-factors with either a larger value of the spin−orbit coupling ($\lambda = -1200\ cm^{-1}$) or smaller values values for *D* and *E* and excitation energies of the LF states.

Table 4. *g*-Factors in the Monomer and the Dimer

	monomer	dimer
g_x	1.50	1.54
g_y	2.79	2.76
g_z	2.40	2.47

In this section, it has been shown that *g*-factors calculated with the MS-CASPT2/SO-RASSI wave function compares well to the experimental values, especially in the *y* and *z*

(58) Ko, J.; Zhang, L.-T.; Ondrechen, M. J. *J. Am. Chem. Soc.* **1986**, *108*, 1712.
(59) Golding, R. M. *Applied wave mechanics*; Van Nostrand: New York, 1969.

directions; these latter factors are mainly due to first-order interaction with the ground state while g_x is due to the interaction between the excited states. Finally, *g*-factors of the CT ion are shown to be independent of the coupling between the centers and to be the same as in the monomer because the coupling acts in a symmetry different from the one of the ground state. This discussion supposes a center of symmetry for the molecule that disappears with the rotation of the ammonia, but the coupling between states of symmetry gerade and ungerade induced by small changes in the structure of the molecule will be negligible and will not change the previous conclusions.

4. Conclusions

The mixed-valence compound $[(NH_3)_5-Ru-pyrazine-Ru-(NH_3)_5]^{5+}$ has been studied using the CASSCF/ CASPT2 method. It has been shown that the ground state is poorly described at the SCF step because this method overestimates the weight of the configuration with one electron in the π^* orbital. A method that reconsiders the zeroth-order wave function after calculation of the dynamical correlation like MS-CASPT2 is needed. With one of the CAS, the coupling between the two configurations seem to be slightly overestimated, leading to a ground state that is 3000 cm^{-1} too low so that the energy of all the transitions is overestimated by this energy, except LF ones; thus, the intervalence band energy is well reproduced. The full excited-states spectrum has been calculated and analyzed: 350 states were found below 50 000 cm^{-1} and from 20 000 cm^{-1}, the states form a quasi-continuum with metal centered transitions, MLCT to the second π^* and $\pi \rightarrow \pi^*$ transitions. To assign the theoretical bands to the experimental ones, transition dipole moments have been calculated for the UV−visible spectroscopy as usually done, and C terms MCD transition moments have been calculated on wave functions including spin−orbit coupling as explained in the Appendix. To the best of our knowledge, it is the first time that such transition moments have been determined. All the experimental bands have been assigned, the assignment of two of the bands highest in energy being different from previous works. There is a shift of 3000 cm^{-1} as mentioned above. Furthermore, this shift is strongly dependent on basis set and active space. The analysis of the LF states of both the monomer and the dimer shows that the one-center axial distortion is due to the destabilization of the d_{xz} orbital by interaction with a π orbital of the pyrazine while the coupling between the two centers is due to the stabilization of the ungerade combination of the d_{xz} orbitals by interaction with a π^* orbital of the pyrazine. Our analysis permits a full understanding of the origin of the axial and rhombic distortion parameters *D* and *E*; none of the many previous theoretical works had analyzed the origin of these two parameters because all the authors were focusing on only three orbitals, the two d_{xz} and π^*. The evaluation of *D* and *E* from LF transitions is in agreement with the ones fitting the EPR spectra as proposed by Fürholz et al.[50]

Furthermore, *g*-factors have been determined from ab initio calculations without any a priori model; the ab initio determination of the anisotropy of the g-matrix in bimetallic species has started very recently with DFT calculations,[30,31,32] and to our knowledge, ours is the first attempt with wave function-based theory. Our results for the anisotropy of the *g*-matrix compare very well in the directions perpendicular to the intermetallic axis: the anisotropy is due to direct interaction of the spin-free ground state with an LF excited state, while the spin contribution is quite important and reduces the anisotropy. On the other hand, the effect is underestimated parallel to the axis: in this direction, there is no direct interaction between the ground state and a low-lying excited-state, and the orbital contribution is due to the interaction between the two LF excited states; the spin contribution is important as well and emphasizes the anisotropy in this direction. It is interesting to note that *g*-factors calculated in our previous article are systematically underestimated as well when they are of second order, that is, when there is no direct orbital interaction between the ground and the excited states. The model that comes out from our calculations is consistent with the previous works except that we have taken into account the symmetry relying the two metallic centers. Solving the model using eq 4 is much easier that the previous procedures, and it is easy to show that the *g*-factors of the CT ion are independent of the electronic coupling V_{AB} between the metallic centers and are therefore the same as in the monomers; this is confirmed by calculating the *g*-matrix in the monomer.

The CT ion has been the prototype of the mixed-valence compound: we chose this molecule because of the abundance of the experimental data and previous calculations. The low energy of the first π^* orbital of the bridge induces the large electronic coupling between the metallic coupling but makes its description more difficult; the use of wave function-based theory permits the full description of all the excited states, most of them being by far not monodeterminental. Finally, the use of EPR spectroscopy is widely used as fingerprints of bimetallic and polymetallic species, especially in biological systems, and the total *g*-matrix is evaluated as a linear combination of the local *g*-matrix using the vector coupling scheme. This work opens the doors to the analysis of *g*-matrices in such compounds without the use of a priori models.

Appendix

The difference of molar extinction coefficients of the *f*-th transition at energy $\tilde{\nu}$ for left-handed and right-handed circularly polarized light for a compound in a magnetic field $\vec{B}$ parallel to the *z* axis, when keeping only terms linear in B_z is given by[60,61]

$$\epsilon_L(\tilde{\nu}) - \epsilon_R(\tilde{\nu}) = \frac{-16\pi^3 \mathcal{N}\tilde{\nu}}{2303 \times 3h^2c^2} B_z \left\{ \frac{\partial g'(\tilde{\nu})}{\partial \tilde{\nu}} \mathcal{A}_z(0f) + g'(\tilde{\nu}) \left[\mathcal{B}_z(0f) + \mathcal{C}_z(0f) \frac{hc}{kT} \right] \right\} \quad (13)$$

(60) Buckingham, A. D.; Stephens, P. J. *Ann. Rev. Phys. Chem.* **1966**, *17*, 399.
(61) Michl, J.; Thulstrup, E. W. *Spectroscopy with polarized light*; Wiley-VCH: New York, 1995.

where $g'(\tilde{\nu})$ is the line-shape function, T is temperature, $\hbar$ is Planck's constant, c is the speed of light, $\mathcal{N}$ is Avogadro's constant, and

$$\mathcal{A}_z(0f) = \frac{3i}{2d}\sum_{\kappa_0\kappa_f}[m_z(\Phi_f^{z;\kappa_f}\Phi_f^{z;\kappa_f}) - m_z(\Phi_0^{z;\kappa_0}\Phi_0^{z;\kappa_0})] \\ [\vec{\mu}(\Phi_0^{z;\kappa_0}\Phi_f^{z;\kappa_f}) \wedge \vec{\mu}(\Phi_f^{z;\kappa_f}\Phi_0^{z;\kappa_0})]_z \quad (14)$$

$$\mathcal{B}_z(0f) = \\ \frac{3}{d}\sum_{\kappa_0\kappa_f}\mathrm{Im}\left\{\sum_{j(j\neq 0)}\frac{m_z(\Phi_j^z\Phi_0^{z;\kappa_0})}{\tilde{\nu}_j}[\vec{\mu}(\Phi_f^{z;\kappa_f}\Phi_j^z) \wedge \vec{\mu}(\Phi_0^{z;\kappa_0}\Phi_f^{z;\kappa_f})]_z + \right. \\ \left. \sum_{j(j\neq f)}\frac{m_z(\Phi_f^{z;\kappa_f}\Phi_j^z)}{\tilde{\nu}_j - \tilde{\nu}_f}[\vec{\mu}(\Phi_j^z\Phi_0^{z;\kappa_0}) \wedge \vec{\mu}(\Phi_0^{z;\kappa_0}\Phi_f^{z;\kappa_f})]_z\right\} \quad (15)$$

$$\mathcal{C}_z(0f) = \frac{3i}{2d}\sum_{\kappa_0\kappa_f} m_z(\Phi_0^{z;\kappa_0}\Phi_0^{z;\kappa_0})\,[\vec{\mu}(\Phi_0^{z;\kappa_0}\Phi_f^{z;\kappa_f}) \wedge \vec{\mu}(\Phi_f^{z;\kappa_f}\Phi_0^{z;\kappa_0})]_z \quad (16)$$

where $m_u(\Phi_i\Phi_j) = \langle\Phi_i|\hat{m}_u|\Phi_j\rangle$, $\vec{\mu}(\Phi_i\Phi_j) = \langle\Phi_i|\vec{\mu}|\Phi_j\rangle$, $\hat{m}_u$ is the projection of the magnetic dipole operator on the u axis and $\vec{\mu}$ is the electric dipole operator, d is the degeneracy of the ground state, κ_0 and κ_f run overall the components of the ground state and the f-th state, respectively (if they are degenerate). The superscript z shows that the wave function is an eigenvector of $\hat{m}_z$, and this condition has to be fulfilled for the ground state for eqs 14−16 to be valid.

The numbers $\mathcal{A}(0f)$, $\mathcal{B}(0f)$, and $\mathcal{C}(0f)$, the so-called A, B, and C Faraday terms, characterize the contribution of the $0 \rightarrow f$ transition to the MCD effect as measured on an assembly of identically oriented molecules and are referred to the A, B, and C terms of the $0 \rightarrow f$ transition in the oriented sample. Coriani et al. have calculated the B terms with ab initio techniques,[27] but to the best of our knowledge, the C term has never been deduced from ab initio calculations. All transitions detected by the MCD technique in the CT ion were analyzed to be C term contributions, so we will only focus on this term. The C terms of the $0 \rightarrow f$ transition in directions x and y comes out immediately from eq 16 as

$$\mathcal{C}_x(0f) = \frac{3i}{2d}\sum_{\kappa_0\kappa_f} m_x(\Phi_0^{x;\kappa_0}\Phi_0^{x;\kappa_0})\,[\vec{\mu}(\Phi_0^{x;\kappa_0}\Phi_f^{x;\kappa_f}) \wedge \\ \vec{\mu}(\Phi_f^{x;\kappa_f}\Phi_0^{x;\kappa_0})]_x$$

$$\mathcal{C}_y(0f) = \frac{3i}{2d}\sum_{\kappa_0\kappa_f} m_y(\Phi_0^{y;\kappa_0}\Phi_0^{y;\kappa_0})\,[\vec{\mu}(\Phi_0^{y;\kappa_0}\Phi_f^{y;\kappa_f}) \wedge \\ \vec{\mu}(\Phi_f^{y;\kappa_f}\Phi_0^{y;\kappa_0})]_y \quad (17)$$

where the ground and the f-th states are now expressed as a set of eigenvectors of $\hat{m}_x$ and $\hat{m}_y$, respectively. There is no restriction on the spin part of the excited states, but for convenience they will be expressed as eigenvectors of $\hat{m}_x$ and $\hat{m}_y$ as well. In the CT ion, all the states are Kramers doublets, $\vec{\mu}(\Phi_0^{u;\kappa_0}\Phi_f^{u;\kappa_f})$ and $\vec{\mu}(\Phi_f^{u;\kappa_f}\Phi_0^{u;\kappa_0})$ ($u = x, y, z$) are collinear and there is no contribution to the C term as long as spin−orbit coupling is not included. Orbital contributions to the magnetic moment are neglected, thus $\hat{m}_u = -\mu_B g_e \hat{S}_u$ where μ_B is the Bohr magneton, g_e is the Landé factor of the free electron, and $\hat{S}_u$ is the projection on u axis of the total spin angular momentum operator. When the quantization axis is along z axis, the two spinors describing the Kramers doublet of the I-th state have the form

$$|\Phi_I^z\rangle = |\Phi_I^1;+\rangle_z + i|\Phi_I^2;+\rangle_z + |\Phi_I^3;-\rangle_z + i|\Phi_I^4;-\rangle_z$$

$$|\overline{\Phi_I^z}\rangle = -|\Phi_I^3;+\rangle_z + i|\Phi_I^4;+\rangle_z + |\Phi_I^1;-\rangle_z - i|\Phi_I^2;-\rangle_z \quad (18)$$

where $|\Phi_I^n;\pm\rangle_z$ is a product of a real function Φ_I^n of space coordinates and $|\pm\rangle_u$ a spin eigenvector of $\hat{S}_u$ with eigenvalues $\pm\hbar/2$. The operator in the spin space associated to the rotation of angle θ around $\vec{u}$ axis can be written[62]

$$\mathcal{R}_{\vec{u}}(\theta) = \cos\left(\frac{\theta}{2}\right) - i\vec{\sigma}\cdot\vec{u}\,\sin\left(\frac{\theta}{2}\right)$$

where $\vec{\sigma}$ denotes the set of the three Pauli matrices. The rotation exchanging x (or y) and z is the rotation of angle π around $(\vec{\imath} + \vec{k})/\sqrt{2}$ (or $(\vec{\jmath} + \vec{k})/\sqrt{2}$) where $\vec{\imath}$, $\vec{\jmath}$, and $\vec{k}$ are unit vectors along x, y, and z axis, and the corresponding operator is

$$\mathcal{R}_x = \frac{i}{\sqrt{2}}\begin{bmatrix}1 & 1\\ 1 & -1\end{bmatrix}$$

or

$$\mathcal{R}_y = \frac{i}{\sqrt{2}}\begin{bmatrix}1 & -i\\ i & -1\end{bmatrix}$$

Finally, the two spinors describing the I-th state can be written as eigenvectors of $\hat{S}_x$

$$|\Phi_I^x\rangle = \frac{i}{\sqrt{2}}(\mathcal{R}_x|\Phi_I^z\rangle + \mathcal{R}_x|\overline{\Phi_I^z}\rangle) = |\Phi_I^1;+\rangle_x + i|\Phi_I^4;+\rangle_x - \\ |\Phi_I^3;-\rangle_x + i|\Phi_I^2;-\rangle_x$$

$$|\overline{\Phi_I^x}\rangle = \frac{i}{\sqrt{2}}(\mathcal{R}_x|\Phi_I^z\rangle - \mathcal{R}_x|\overline{\Phi_I^z}\rangle) = |\Phi_I^3;+\rangle_x + i|\Phi_I^2;+\rangle_x + \\ |\Phi_I^1;-\rangle_x - i|\Phi_I^4;-\rangle_x \quad (19)$$

or as eigenvectors of $\hat{S}_y$

$$|\Phi_I^y\rangle = \frac{1}{\sqrt{2}}(i\mathcal{R}_y|\Phi_I^z\rangle - \mathcal{R}_y|\overline{\Phi_I^z}\rangle) = |\Phi_I^1;+\rangle_y - i|\Phi_I^3;+\rangle_y - \\ |\Phi_I^2;-\rangle_y - i|\Phi_I^4;-\rangle_y$$

$$|\overline{\Phi_I^y}\rangle = \frac{1}{\sqrt{2}}(\mathcal{R}_y|\Phi_I^z\rangle - i\mathcal{R}_y|\overline{\Phi_I^z}\rangle) = |\Phi_I^2;+\rangle_y - i|\Phi_I^4;+\rangle_y + \\ |\Phi_I^1;-\rangle_y + i|\Phi_I^3;-\rangle_y \quad (20)$$

Equations 19 and 20 allow the easy deduction of Kramers doublets for quantization axis along x and y axis from

(62) Cohen-Tannoudji, C.; Diu, B.; Laloë, F. *Mécanique quantique*; Hermann: Paris, 1977.
(63) Dubicki, L.; Ferguson, J.; Krausz, E. R. *J. Am. Chem. Soc.* **1985**, *107*, 179.

Kramers doublets, with the quantization axis along z axis usually provided by calculations. After simplification, eqs 16 and 17 can be written with $u = x, y, z$

$$\mathcal{G}_u(0f) = -3\mu_B g_e S_u(\Phi_0^u \Phi_0^u)\,[\mathrm{Im}\{\vec{\mu}(\Phi_0^u \Phi_f^u)] \wedge \mathrm{Re}\{\vec{\mu}(\Phi_0^u \Phi_f^u)\} - \mathrm{Im}\{\vec{\mu}(\Phi_0^u \overline{\Phi_f^u})\} \wedge \mathrm{Re}\{\vec{\mu}(\Phi_0^u \overline{\Phi_f^u})\}]_u \quad (21)$$

Acknowledgment. The author thanks Trond Saue for critical reading of the manuscript. Calculations have been carried out at CURRI and HPC computing centers in Strasbourg.

IC060816M